Supporting Information

for

Silylation of Iron-Bound Carbon Monoxide

Affords a Terminal Fe Carbyne

*Yunho Lee and Jonas C. Peters**

Division of Chemistry and Chemical Engineering, California Institute of Technology, Pasadena, California 91125 (USA),
and Department of Chemistry, Massachusetts Institute of Technology, Cambridge, Massachusetts 02139 (USA)

Contents

Figure S1. ^{1}H-NMR spectrum (C_6D_6, ppm) of (SiP^{iPr}_3)Fe(CO) (**1**) measured at room temperature.

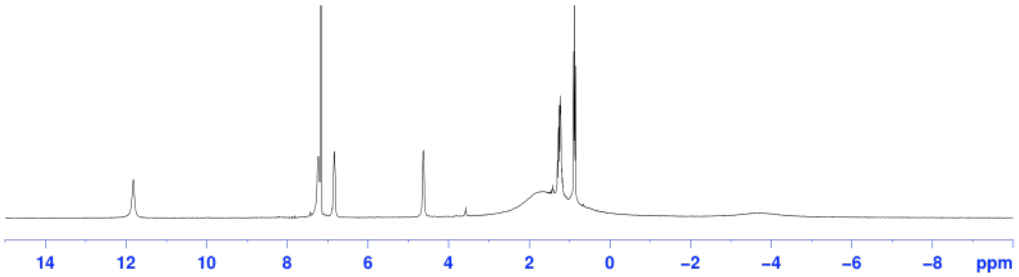

Figure S2. Cyclic voltammogram of (SiP^{iPr}_3)Fe(CO) (**1**) with scan rates: 100, 300, and 500 mV/s. $Fe^{II/I}$ couple at –0.68 V and $Fe^{I/0}$ couple at –1.93 V vs. Fc/Fc^{+} were observed in THF with 0.3 M tetra-*n*-butylammonium hexafluorophosphate as an electrolyte.

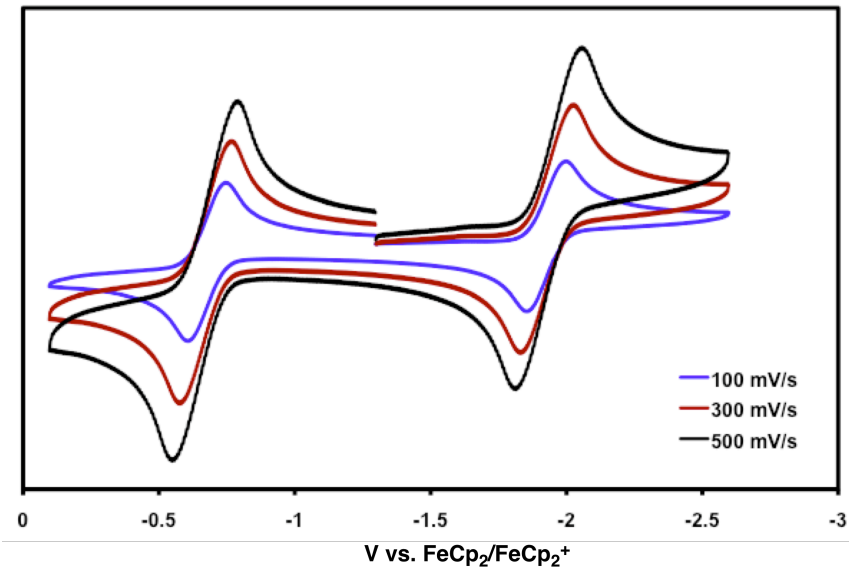

Figure S3. ^{1}H-NMR spectrum (THF-d_8, ppm) of (SiP$^{i\text{Pr}}_3$)Fe{CONa(THF)$_3$} (**2**) measured at room temperature.

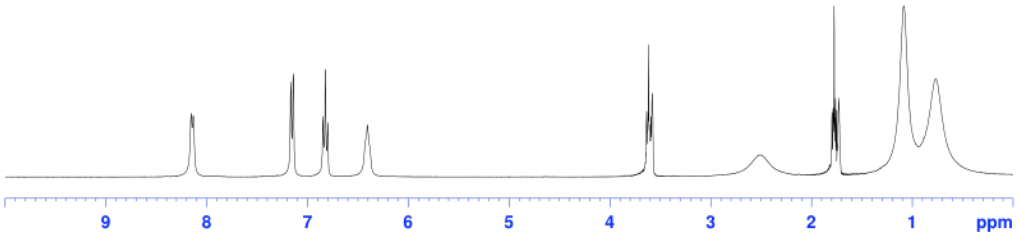

Figure S4. ^{31}P-NMR spectrum (THF-d_8, ppm) of (SiP$^{i\text{Pr}}_3$)Fe{CONa(THF)$_3$} (**2**) measured at –70 °C.

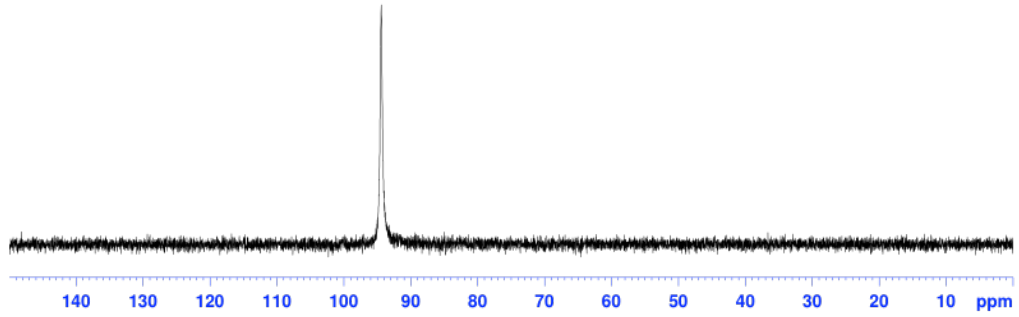

Figure S5. ^{13}C-NMR spectrum (THF-d_8, ppm) of (SiP$^{i\text{Pr}}_3$)Fe{^{13}CONa(THF)$_3$} (**2-^{13}CO**) measured at –70 °C.

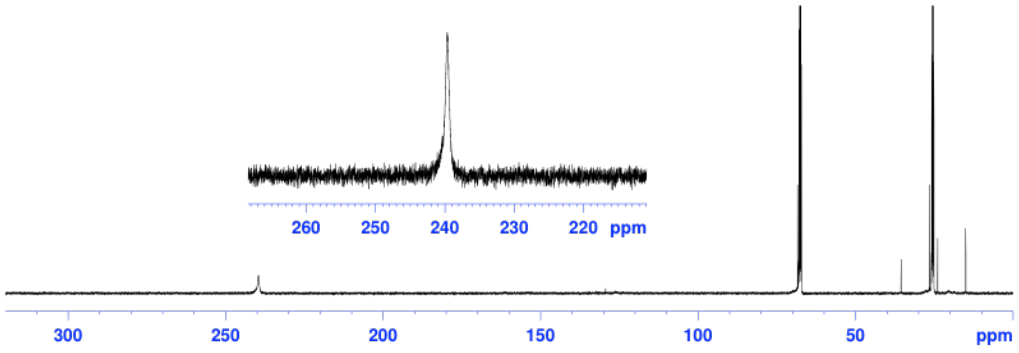

Figure S6. ^{1}H-NMR spectrum (C_6D_6, ppm) of (SiP^{iPr}_3)Fe($COSiMe_3$) (**4**) measured at room temperature.

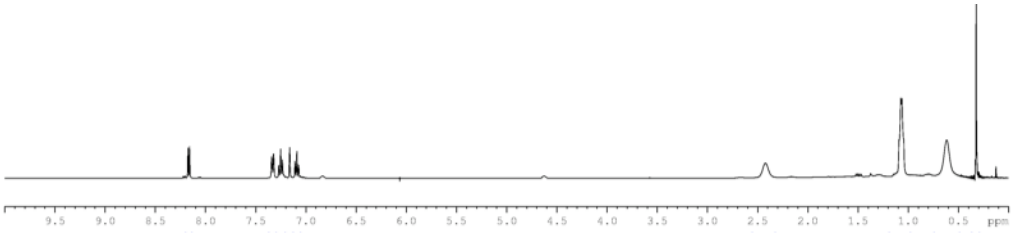

Figure S7. ^{31}P-NMR spectrum (C_6D_6, ppm) of (SiP^{iPr}_3)Fe($^{12}COSiMe_3$) (**4-^{12}CO**) measured at room temperature.

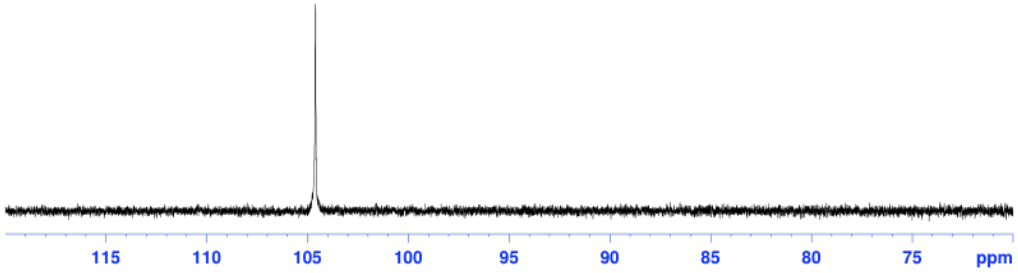

Figure S8. ^{31}P-NMR spectrum (C_6D_6, ppm) of (SiP^{iPr}_3)Fe($^{13}COSiMe_3$) (**4-^{13}CO**) measured at room temperature.

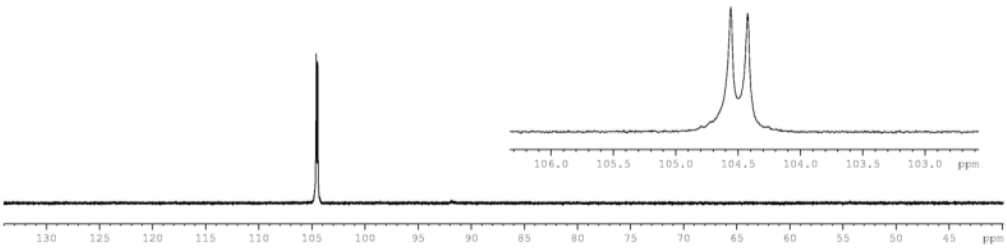

Figure S9. ^{13}C-NMR spectrum (C_6D_6, ppm) of (SiP^{iPr}_3)Fe($^{13}COSiMe_3$) (**4-^{13}CO**) measured at room temperature.

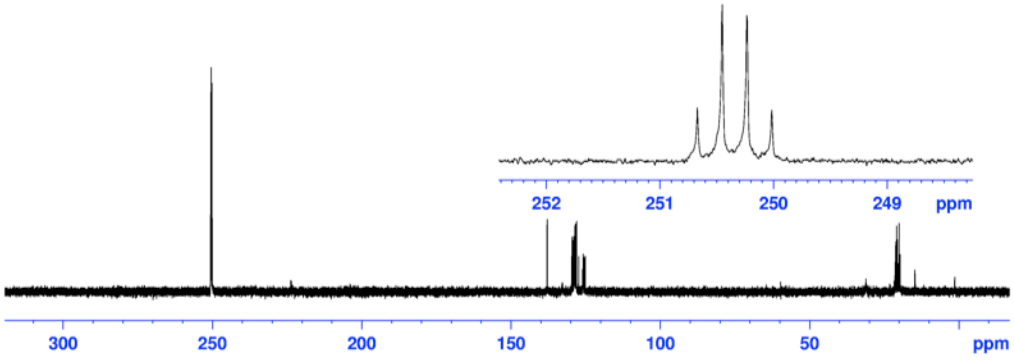

Figure S10. ^{29}Si-NMR spectra (C_6D_6, ppm) of (SiP^{iPr}_3)Fe($COSiMe_3$) (**4**, top) and (SiP^{iPr}_3)Fe($^{13}COSiMe_3$) (**4-^{13}CO**, bottom) measured at room temperature.

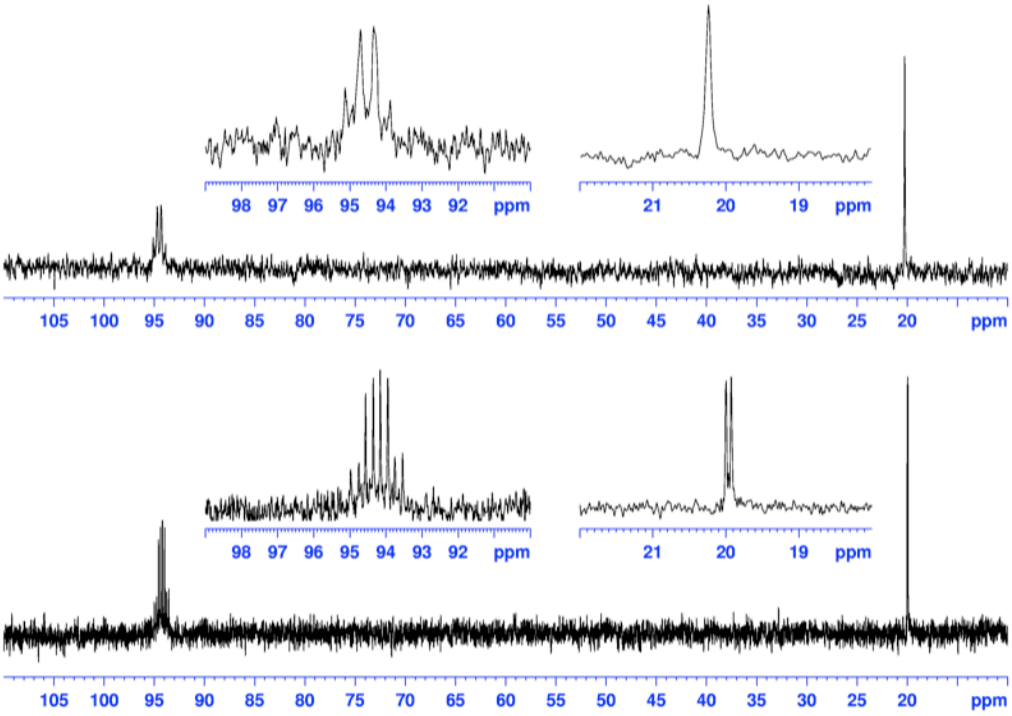

Figure S11. ^{1}H-NMR spectrum (C_6D_6, ppm) of (SiP$^{i\mathrm{Pr}}{}_3$)Fe(COSi^{i}Pr$_3$) measured at room temperature.

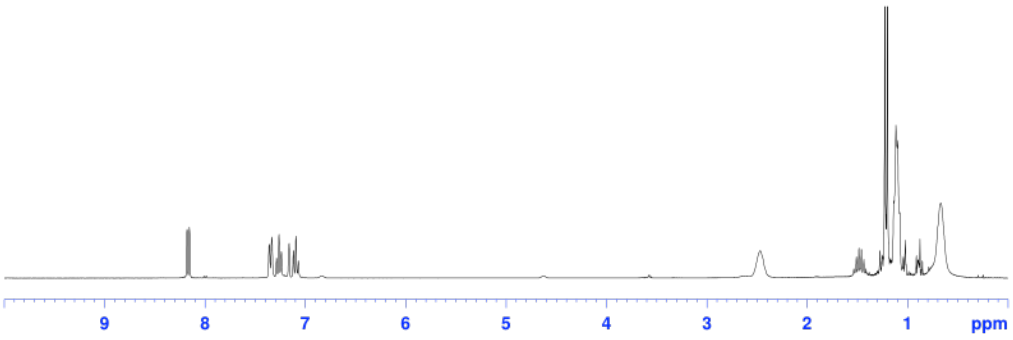

Figure S12. ^{31}P-NMR spectrum (C_6D_6, ppm) of (SiP$^{i\mathrm{Pr}}{}_3$)Fe(COSi^{i}Pr$_3$) measured at room temperature.

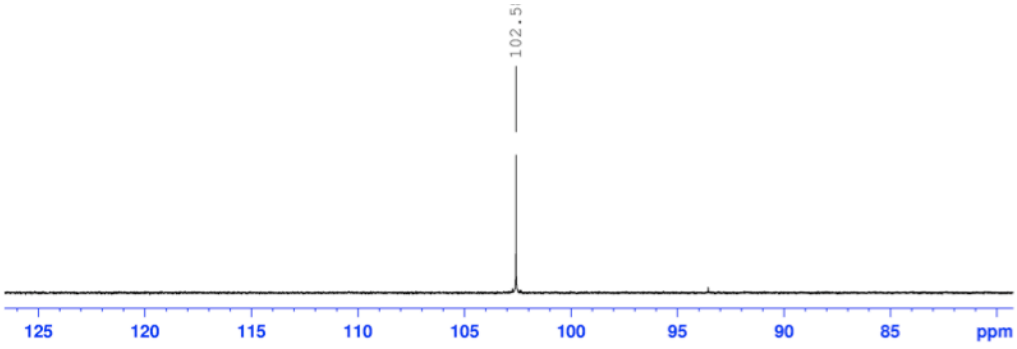

Figure S13. ^{29}Si-NMR spectra (C_6D_6, ppm) of (SiP$^{i\mathrm{Pr}}{}_3$)Fe(COSi^{i}Pr$_3$) (top) and ^{i}Pr$_3$SiOTf (bottom) measured at room temperature.

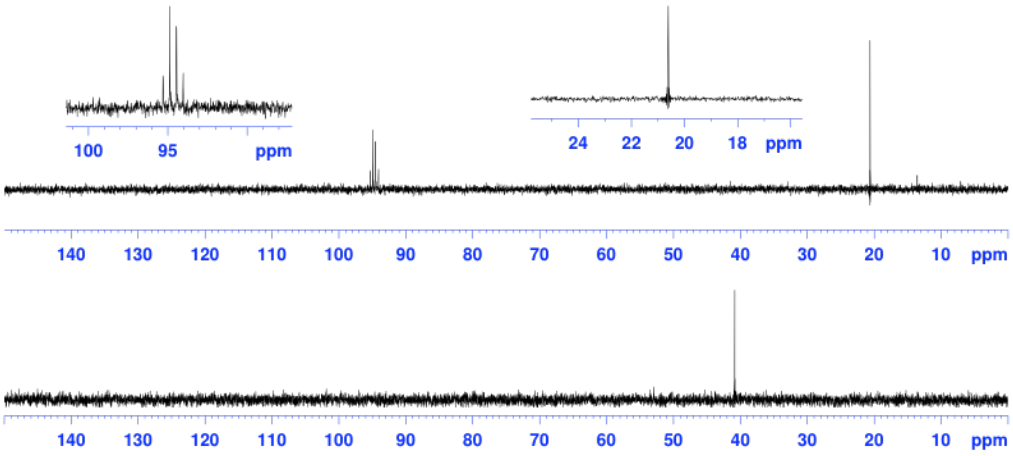

Figure S14. X-ray structure for (SiP$^{i\mathrm{Pr}}_3$)Fe(CO) (**1**). Hydrogen atoms, and one benzene co-solvent molecule are omitted for clarity.

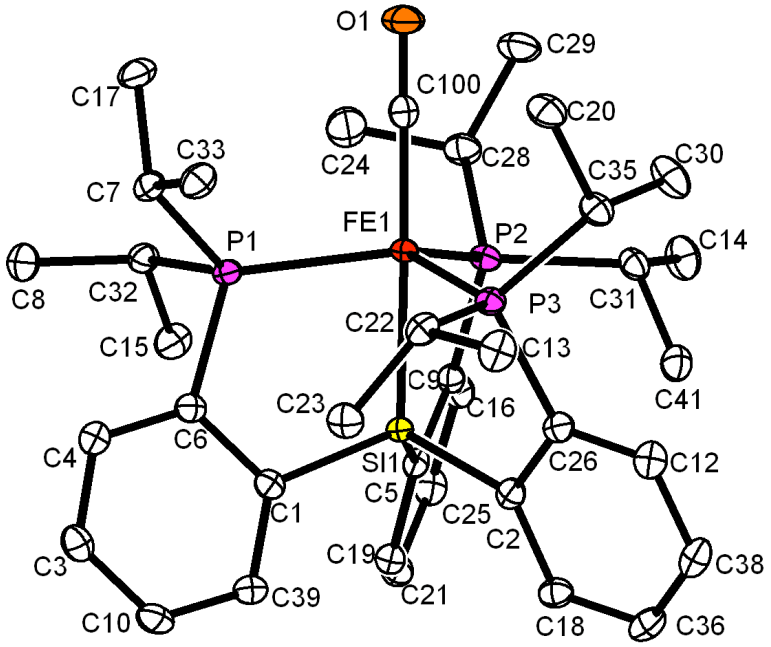

Figure S15. X-ray structure for $(SiP^{iPr}_3)Fe\{CONa(THF)_3\}$ (**2**). Hydrogen atoms are omitted for clarity.

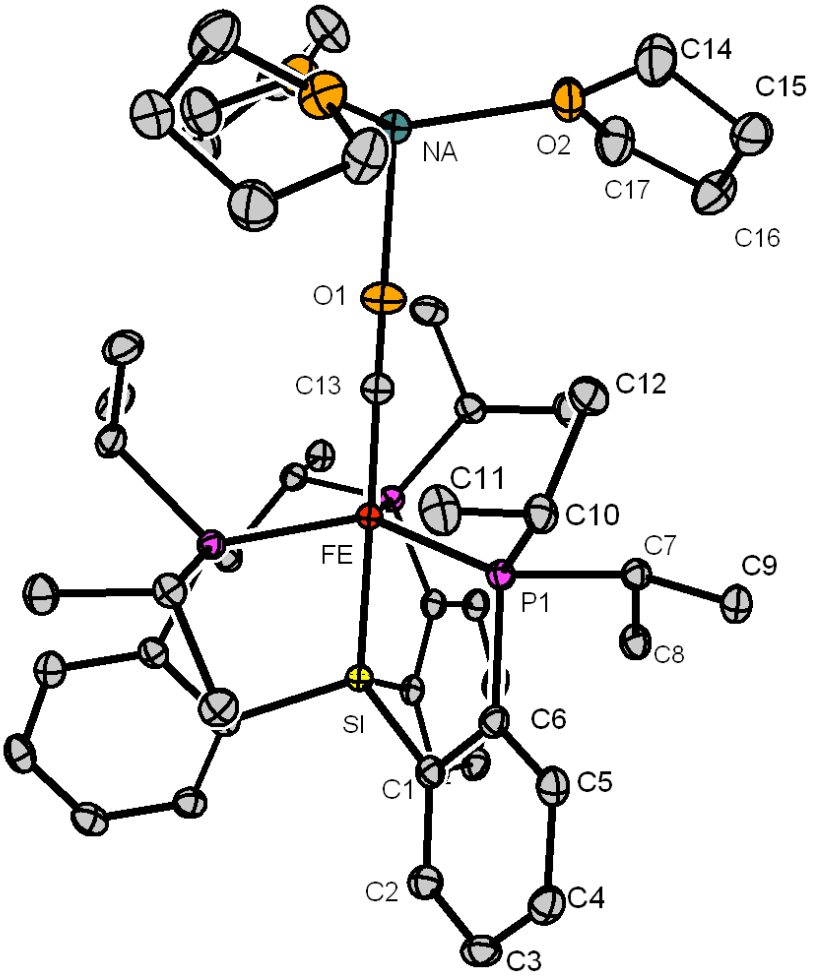

Figure S16. X-ray structure for (SiP$^{i\mathrm{Pr}}_3$)Fe(COSiMe$_3$) (**4**). Hydrogen atoms are omitted for clarity.

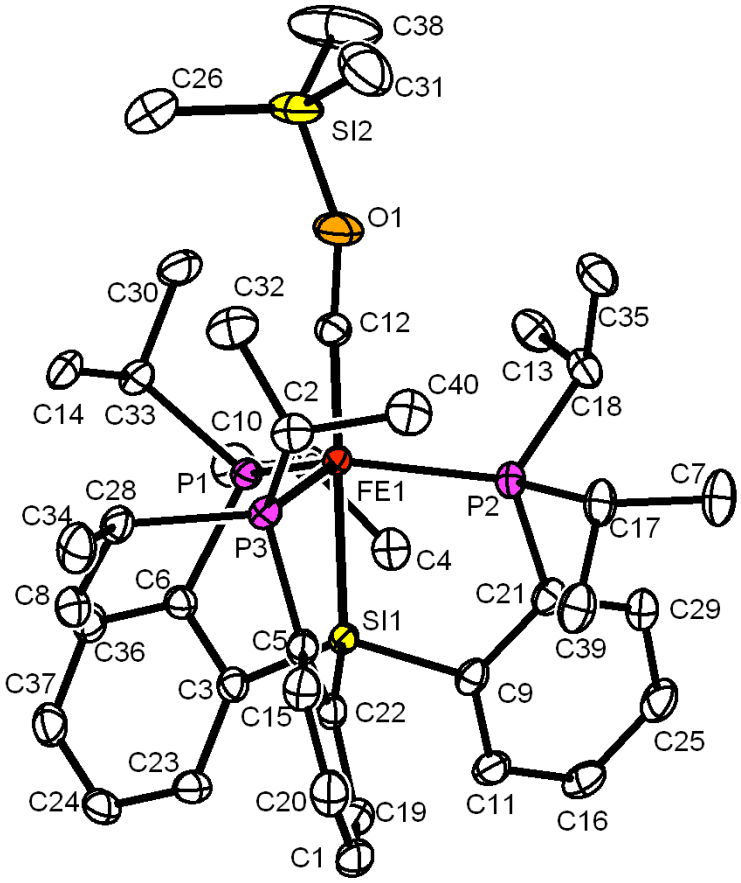

Figure S17. X-ray structure for $\{(SiP^{iPr}_3)Fe(CO)\}\{B(3,5\text{-}(CF_3)_2\text{-}C_6H_3)_4\}$ (**5**). Hydrogen atoms are omitted for clarity.

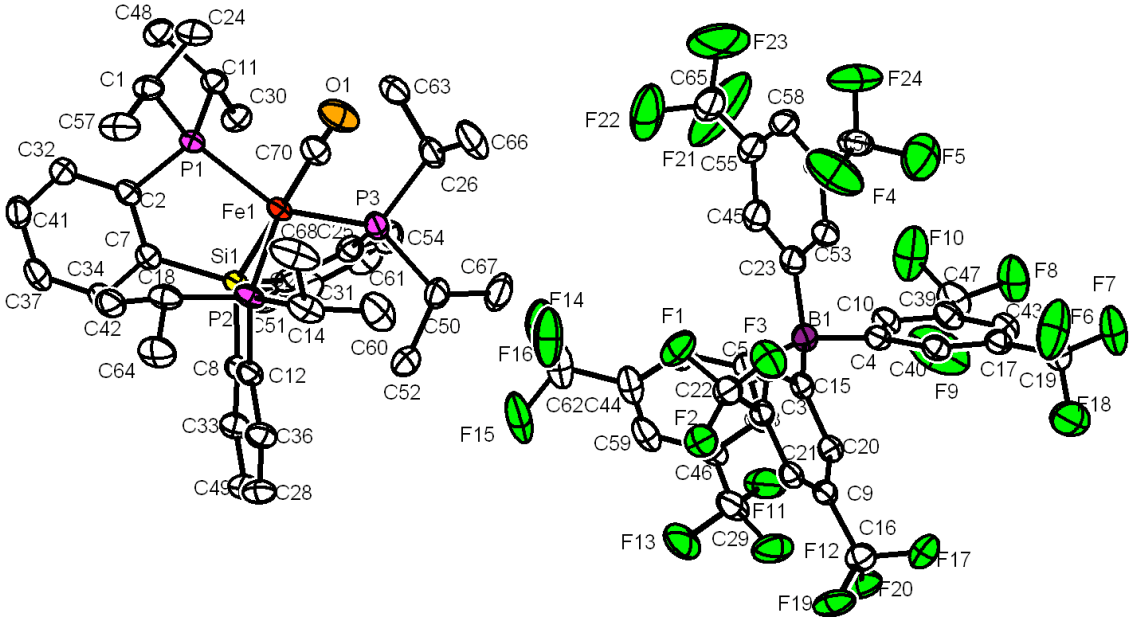

Table S1. Selected bond distances and angles for **1**, **2**, **4** and **5** (Å and °).

	$FeCO^+$ **5**	FeCO **1**	$FeCO^-$ **2**	$FeCOSiMe_3$ **4**
d_{CO}	1.102(4)	1.169(2)	1.188(3)	1.278(3)
d_{FeC}	1.842(3)	1.769(2)	1.732(3)	1.671(2)
d_{FeSi}	2.3245(7)	2.2942(4)	2.2586(8)	2.2973(6)
d_{FeP}	2.3815(8) 2.3894(7) 2.4004(8)	2.2620(4) 2.2752(4) 2.2909(4)	2.1864(4)	2.2182(6) 2.2246(6) 2.2288(6)
∠COX	–	–	180.000(1)	155.0(2)
∠FeCO	178.1(3)	179.7(2)	180.000(1)	173.8(2)
∠SiFeC	178.69(9)	178.04(5)	180.000(1)	177.90(7)
∠PFeP	117.26(3) 119.08(3) 116.94(3)	117.63(2) 114.88(2) 120.91(2)	118.168(6) 118.168(6) 118.169(6)	119.26(2) 115.91(2) 116.76(2)
τ	0.99	0.95	1	0.98

Figure S18. X-band EPR spectrum of **1-^{12}CO** (blue), **1-^{13}CO** (red) and simulation (black) in 2-MeTHF at 77 K.

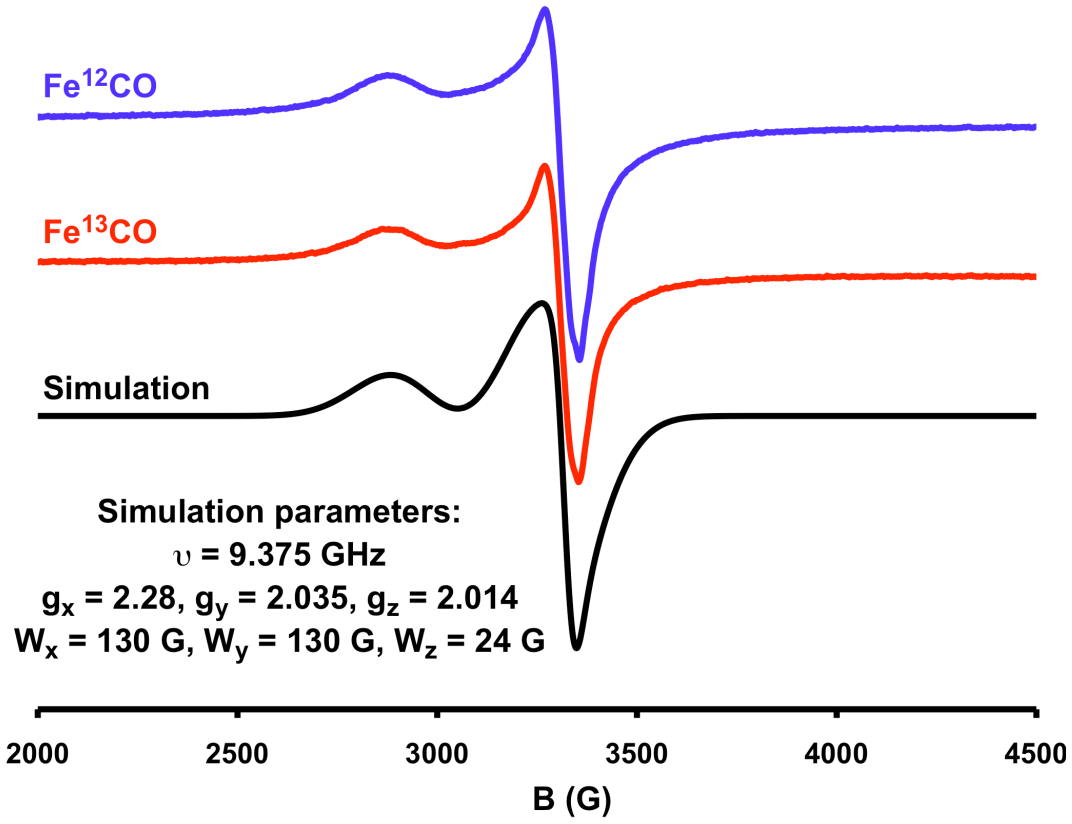

Figure S19. Electronic structures for **2** and **4** from the single point DFT calculations.

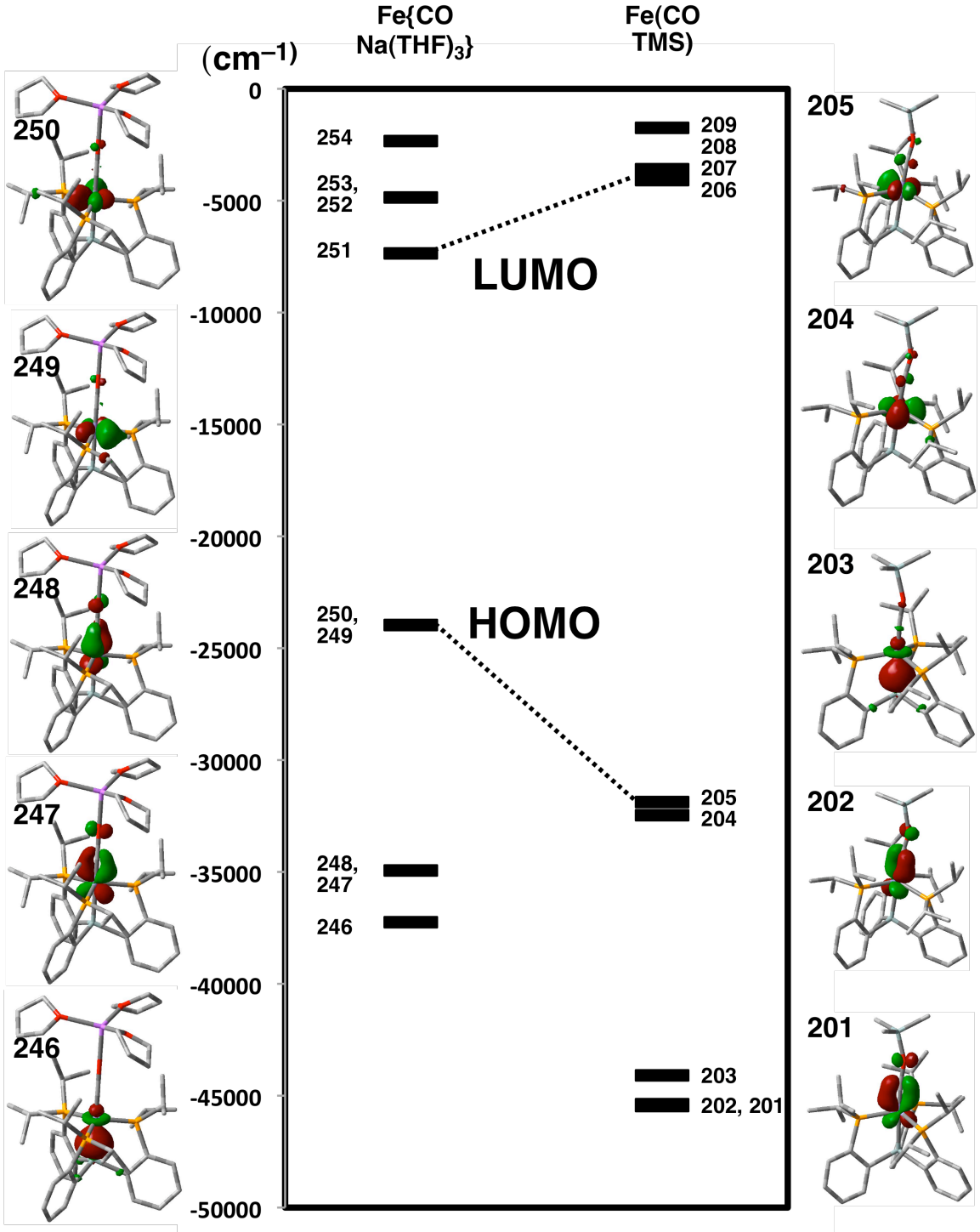

** Lobal representations correspond to the orbitals indicated by the number with 0.07 isocontours.*

Table S2. Selected bond indices and bond orbital occupancies for **2** and **4** from NBO analysis.

	Fe{CONa(THF)$_3$} (**2**)	FeCOTMS (**4**)
Wiberg Bond Index		
Fe-C	1.4845	1.8569
C-O	1.6177	0.6766*
O-Na or Si	0.0384	0.5236
Fe-Si	0.7115	0.7808
Bond Orbital Occupancy		
Fe-C	1.85804 (34.37 % Fe, 65.63 % C)	1.88259 (35.86 % Fe, 64.14 % C) 1.73379 (67.84 % Fe, 32.16 % C) 1.73122 (69.19 % Fe, 30.81 % C)
C-O	1.99089 (27.53 % C, 72.47 % O)	1.98781 (22.88 % C, 77.12 % O)
Fe-Si	1.61800 (55.48 % Fe, 44.52 % Si)	1.64338 (59.08 % Fe, 40.92 % Si)
Fe-P	1.80671 (30.59 % Fe, 69.41 % P) 1.80666 (30.59 % Fe, 69.41 % P) 1.80667 (30.59 % Fe, 69.41 % P)	1.84533 (35.09 % Fe, 64.91 % P) 1.84533 (35.15 % Fe, 64.85 % P) 1.84533 (35.35 % Fe, 64.65 % P)
Fe (LP)	1.84666 1.84652 1.67127 1.67118	1.88179 1.88382

* Wiberg Bond Indices of free CO and N_2 reveal 2.1834 and 3.0493, respectively. The bond indices for C≡C and C-O bonds in propynyl tosylate[1] are 2.6761 and 1.0649, respectively. Geometry optimization and natural bond orbital (NBO) analysis for propynyl tosylate were run on the Gaussian03 suite of programs[2] with the B3LYP level of theory with the 6-311G** basis set for all atoms.

[1] Stang, P. J.; Crittell, C. M.; Arif, A. M.; Karni, M.; Apeloig, Y. *J. Am. Chem. Soc*. **1991**, *113*, 7461-7470.

[2] Frisch, M. J.; Trucks, G. W.; Schlegel, H. B.; Scuseria, G. E.; Robb, M. A.; Cheeseman, J. R.; Montgomery, J. A., Jr.; Vreven, T.; Kudin, K. N.; Burant, J. C.; Millam, J. M.; Iyengar, S. S.; Tomasi, J.; Barone, V.; Mennucci, B.; Cossi,M.; Scalmani, G.; Rega, N.; Petersson, G. A.; Nakatsuji, H.; Hada, M.; Ehara, M.; Toyota, K.; Hasegawa, J.; Ishida, M.; Nakajima, T.; Honda, Y.; Kitao, O.; Nakai, H.; Klene, M.; Li, X.; Knox, J. E.; Hratchian, H. P.; Cross, J. B.; Bakken, V.; Adamo, C.; Jaramillo, J.; Gomperts, R.; Stratmann, R. E.; Yazyev, O.; Austin,A. J.; Cammi, R.; Pomelli, C.; Ochterski, J. W.; Ayala, P. Y.; Morokuma, K.; Voth, G. A.; Salvador, P.; Dannenberg, J. J.; Zakrzewski, V. G.; Dapprich, S.; Daniels, A. D.; Strain, M. C.; Farkas, O.; Malick, D. K.; Rabuck, A.

D.; Raghavachari, K.; Foresman, J. B.; Ortiz, J. V.; Cui, Q.; Baboul, A. G.; Clifford, S.; Cioslowski, J.; Stefanov, B. B.; Liu, G.; Liashenko, A.; Piskorz, P.; Komaromi, I.; Martin, R. L.; Fox, D. J.; Keith, T.;M. A. Al-Laham, Peng, C. Y.; Nanayakkara, A.; Challacombe, M.; Gill, P. M. W.; Johnson, B.; Chen, W.; Wong, M. W.; Gonzalez, C.; Pople, J. A. *Gaussian 03, Revision C. 02;Gaussian*, Inc.: Wallingford, CT, **2004**.

Table S3. Mulliken atomic spin densities in the virtual cationic species of **2** and **4**.

	Cationic Fe{CONa(THF)$_3$} (**2**)*	Cationic FeCOTMS (**4**)*
Fe	47.09 %	46.58 %
C	11.69 %	16.75 %
O	2.03 %	1.31 %
Si_{TMS}	–	-1.51 %
P	11.62 %, 3.84 %, -2.72 %	10.31 %, 3.51 %, -5.59 %
Si	18.86 %	13.75 %

* To attempt to crudely assign the relative contribution of atomic orbitals to the HOMO we calculated the Mulliken atomic spin density of a hypothetical $\{4\}^+$. Mulliken atomic spin densities of corresponding virtual cationic species of **2** and **4** were derived from the original single point calculations of each singlet species by assigning **2** and **4** as doublet species without further optimizations.

Table S4. Mulliken atomic spin densities of the multi-cationic virtual species of **4** from $\{\mathbf{4}\}^+$ to $\{\mathbf{4}\}^{9+}$.

	$\{\mathbf{4}\}^+$	$\{\mathbf{4}\}^{3+}$	$\{\mathbf{4}\}^{5+}$	$\{\mathbf{4}\}^{7+}$	$\{\mathbf{4}\}^{9+}$
#[a]	1	3	5	7	9
Fe	0.465835	0.481468	0.380404	0.621371	0.618963
Si	0.137474	0.151904	0.282746	0.025216	0.022492
P	0.103100	-0.040430	0.008950	-0.001927	0.012401
P	0.035122	0.021843	0.019856	-0.009516	0.007213
P	-0.055930	0.151920	0.032625	-0.006322	0.007288
Si_{TMS}	-0.015148	-0.003280	-0.054115	-0.013744	-0.010513
C	0.167536	0.127118	0.087370	0.194103	0.168105
O	0.013079	0.014192	-0.001821	0.062248	0.068138

a: number of electrons taken out from the original calculation of **4**.

Figure S20. X-ray structure for {(SiP$^{i\mathrm{Pr}}_3$)Fe(Cl)}{B(3,5-(CF$_3$)$_2$-C$_6$H$_3$)$_4$}. Hydrogen atoms, and one pentane co-solvent molecule are omitted for clarity.

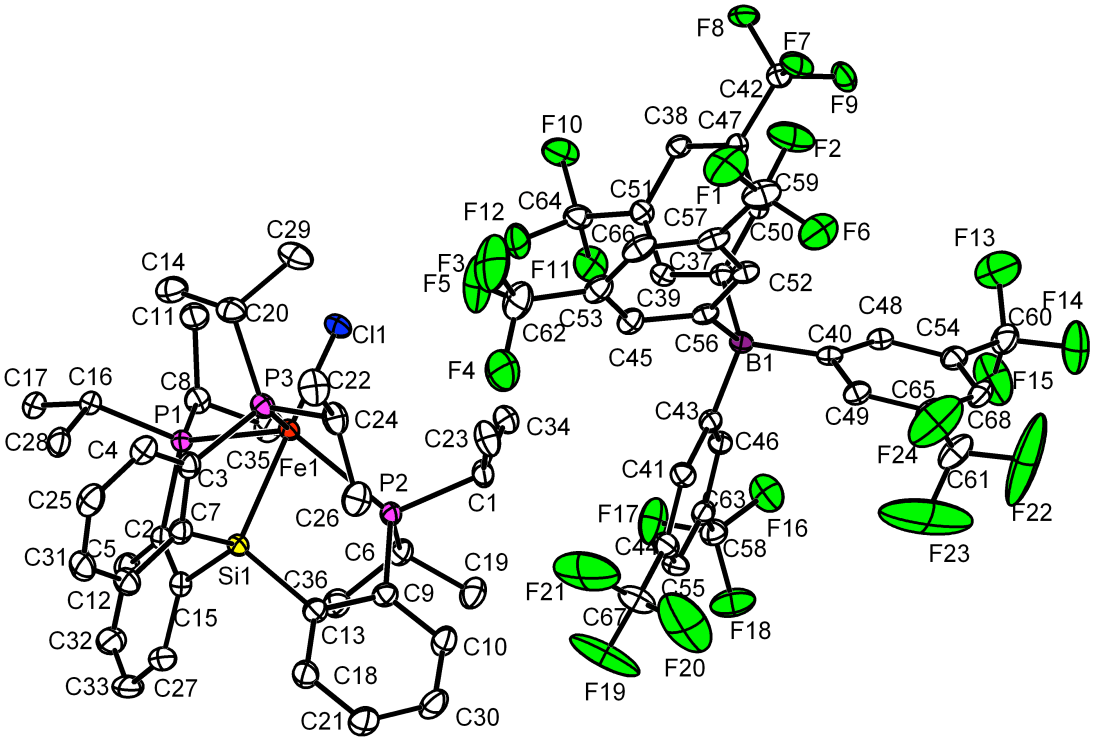

Figure S21. Zero field Mössbauer spectra of (SiP$^{i\mathrm{Pr}}_3$)Fe(C1)[3] (a) and {(SiP$^{i\mathrm{Pr}}_3$)Fe(C1)} {B(3,5-(CF$_3$)$_2$-C$_6$H$_3$)$_4$} (b) at 77 K.

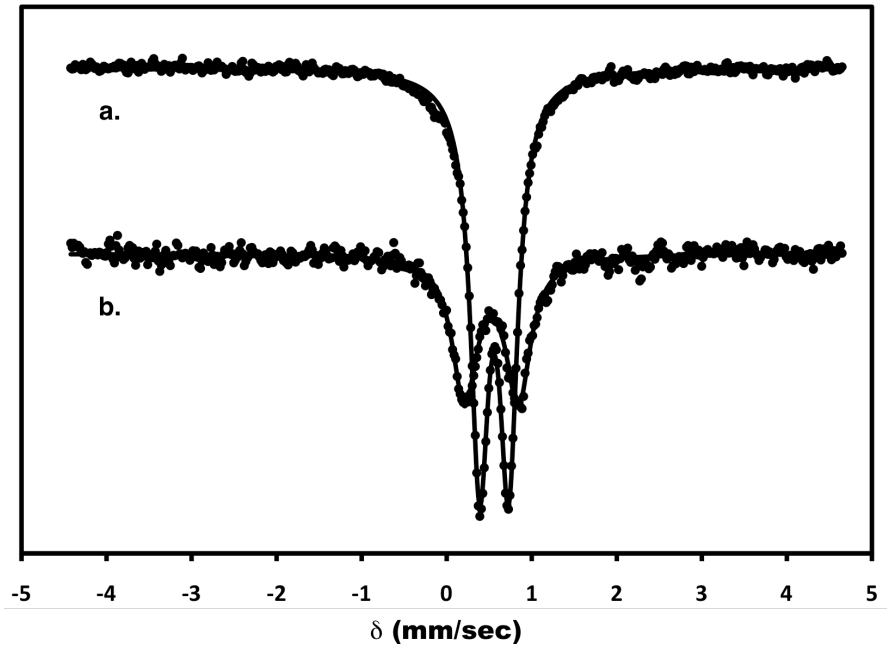

[3] Lee, Y., N. P. Mankad, J. C. Peters, *Nature Chem.* **2010**, 2, 558-565.

Figure S22. Mössbauer spectra of (SiP^{iPr}_3)Fe(CO) (**1**) in zero field (a), parallel (b) and perpendicular (c) magnetic field, 45 mT at 77 K.